



**HAL**  
open science

## Experimental determination of the critical loci for R-23 + (n-propane or n-hexane) and R-116 + n-propane binary mixtures

Mark D. Williams-Wynn, Jamal El Abbadi, Alain Valtz, Elodie Kovacs, Céline Houriez, Paramespri Naidoo, Christophe Coquelet, Deresh Ramjugernath

### ► To cite this version:

Mark D. Williams-Wynn, Jamal El Abbadi, Alain Valtz, Elodie Kovacs, Céline Houriez, et al.. Experimental determination of the critical loci for R-23 + (n-propane or n-hexane) and R-116 + n-propane binary mixtures. *Journal of Chemical Thermodynamics*, 2017, 108, pp.84-96. 10.1016/j.JCT.2016.12.021 . hal-01460064

**HAL Id: hal-01460064**

**<https://minesparis-psl.hal.science/hal-01460064>**

Submitted on 7 Feb 2017

**HAL** is a multi-disciplinary open access archive for the deposit and dissemination of scientific research documents, whether they are published or not. The documents may come from teaching and research institutions in France or abroad, or from public or private research centers.

L'archive ouverte pluridisciplinaire **HAL**, est destinée au dépôt et à la diffusion de documents scientifiques de niveau recherche, publiés ou non, émanant des établissements d'enseignement et de recherche français ou étrangers, des laboratoires publics ou privés.

# Experimental determination of the critical loci for R-23 + (n-propane or n-hexane) and R-116 + n- propane binary mixtures

*Mark D. Williams-Wynn<sup>†</sup>, Jamal el Abbadi<sup>‡</sup>, Alain Valtz<sup>‡</sup>, Elodie Kovacs<sup>‡</sup>, Céline Houriez<sup>‡</sup>,  
Paramespri Naidoo<sup>†</sup>, Christophe Coquelet<sup>‡</sup>, Deresh Ramjugernath<sup>\*†</sup>*

<sup>†</sup>*Thermodynamics Research Unit, School of Engineering, University of KwaZulu-Natal,  
Howard College Campus, King George V Avenue, Durban, 4041, South Africa*

<sup>‡</sup>*MINES ParisTech, PSL Research University, CTP – Centre Thermodynamics of Processes,  
35 Rue Saint Honoré, 77305 Fontainebleau, France*

\*Corresponding author. E-mail: [ramjuger@ukzn.ac.za](mailto:ramjuger@ukzn.ac.za). Tel. +27 31 260 3128. Fax:  
+2731 260 1118.

## **Abstract**

Isothermal VLE for the R-23 + n-propane system was measured using a static-analytic apparatus at temperatures between  $T = (293.18 \text{ and } 353.15) \text{ K}$ . The critical loci for the systems R-23 + (n-propane or n-hexane) and R-116 + n-propane were measured using a critical point determination apparatus. The method of Ungerer et al. was used to extrapolate the isothermal VLE data to the isothermal critical locus. These extrapolated critical loci were compared with experimental data. The Redlich-Kister type correlations were used to correlate the critical loci of the systems. A critical locus curve for the R-23 + n-hexane system which was calculated by the method of Heidemann and Khalil was compared with the experimental critical loci. The systems were classified according to the van Konynenburg and Scott classification system.

**Keywords:** Critical loci; R-23; R-116; n-propane; n-hexane; VLE.

## Introduction

Supercritical fluids exhibit a number of physical properties that give them an advantage over conventional liquid solvents [1]. Most importantly, supercritical fluids have densities that are of a similar magnitude to conventional solvents. However, these densities can be varied substantially by altering the pressure and temperature of the fluid [2]. Carbon dioxide (CO<sub>2</sub>) is by far the most commonly used supercritical solvent [1].

CO<sub>2</sub> is essentially a non-polar solvent, with a dipole moment of zero debye [3]. This inhibits the ability of CO<sub>2</sub> to dissolve polar components to any useful extent [2]. In addition to this, CO<sub>2</sub> does not exhibit very large capacities for solutes, translating into larger volumes of solvent being required to perform a separation. In order to overcome these problems, an alternative solvent or mixture of solvents must be used. The more commonly applied method is the addition of co-solvents to the CO<sub>2</sub>, in order to improve its ability to dissolve polar components [3]. Alternatively, the solvent can be replaced with a more polar solvent. This study continues a previous investigation into the use of trifluoromethane (R-23) and hexafluoroethane (R-116) as supercritical solvents [4].

In this study, the critical loci of three systems, R-23 + (n-propane or n-hexane) and R-116 + n-propane were measured using a critical point determination apparatus, and were compared to values either extrapolated using the method described by Ungerer et al. [5], or calculated using the method of Heidemann and Khalil [6]. Ju et al. [7] measured several isotherms of the R-23 + n-propane system at temperatures of between  $T = (283.15 \text{ and } 313.15) \text{ K}$ . To supplement this data, several additional VLE isotherms were measured for the R-23 + n-propane system using a static-analytic apparatus, and are reported in this work. Both the

VLE measurements and the critical loci measurements were performed at the Centre for Thermodynamics of Processes (CTP).

VLE data for the R-116 + n-propane system were obtained from the work of Ramjugernath et al. [8]. For the R-23 + n-hexane system, the data of Williams-Wynn et al. [4] were used, and for the R-116 + n-hexane, the data that were reported by Ramjugernath et al. [9] were extrapolated to the critical point.

## **Experimental**

**Materials.** The suppliers, CAS numbers and stated purities of the chemicals that were used in this study are listed in Table 1. The critical properties of the components are provided in Table 2.

**Experimental Apparatus.** Two different apparatus were used in this work. A static-analytic apparatus was used to measure the isothermal VLE data for the system R-23 + n-propane, and a critical point determination apparatus was used to measure the critical loci of the three systems.

*Static-analytic apparatus.* The static-analytic apparatus used in this study uses a capillary sampler (ROLSI<sup>TM</sup>) [10] to sample the liquid and vapour phases. The equipment is similar to that depicted in Figure 1, which was used by Juntarachat et al. [11].

The equilibrium cell is submerged into a thermo-regulated liquid bath which is maintained at a constant temperature. The deviations of the temperature within the bath are less than 0.01 K. The temperature of the fluid inside the equilibrium cell is monitored by two platinum resistance thermometer probes (Pt100) connected to a data acquisition unit (HP34970A) [12].

The use of two probes enables any gradients within the cell to be quantified, and the average of the two measurements is used as the measured temperature.

The Pt100 probes were calibrated against a 25  $\Omega$  reference platinum resistance thermometer (Hart Scientific). This Pt25 reference probe was calibrated by the “Laboratoire National d’Essais de Paris” based on the 1990 International Temperature Scale (ITS 90). The maximum error given by the calibration of the reference probes was estimated to be within 0.05 K.

The pressure is measured using one of two pressure transducers (DRUCK, 0 – 3 MPa, 0 – 30 MPa) installed on the apparatus. The choice of pressure transducer is dependent upon the maximum pressures generated by the system being characterised. The two pressure transducers are also connected to the data acquisition unit (HP34970A). The pressure transducers were calibrated against an automated pressure calibrator (GE Sensing, model PACE 5000). The pressure uncertainties from the transducers are estimated to be within 0.2 kPa for the “0 – 3 MPa” pressure transducer and 0.6 kPa for the “0 – 30 MPa” pressure transducer.

The compositions of the phases present within the cell are analysed with a gas chromatograph (VARIAN, model CP-3800), which is equipped with a thermal conductivity detector (TCD). The analytical column within the gas chromatograph (GC) is a PORAPAK Q, 80/100 mesh (Silcosteel tube, length: 2m, diameter: 3.2mm, from Restek).

The response of the TCD is calibrated by introducing known amounts of each pure component into the gas chromatograph, using an automatic syringe. The calibration equation was fitted to relate the response of the TCD to the amount of the component introduced.

*Critical point determination apparatus.* The critical point determination apparatus that was commissioned by Soo et al. [13] at the CTP at Mines ParisTech was modified to measure the critical loci of the three systems. This apparatus was originally a dynamic-synthetic apparatus, but due to the large relative volatilities of the constituent components of the three systems, in particular the systems containing n-hexane, the apparatus was modified to perform static-synthetic measurements. A schematic drawing of this experimental apparatus is shown in Figure 2.

To enable the use of the apparatus of Soo et al. to perform static-synthetic measurements, the heat exchanger was removed from the line of fluid flow. Thus, the major sections of the apparatus are a volumetric press, a syringe pump and an equilibrium cell. A synthetic mixture is prepared in the volumetric press, **VPr**, by mixing known masses of the required components. The volumetric press is attached to an ISCO 260D syringe pump, **SP**. The contents of the volumetric press are forced into the syringe pump, by applying a pressure to the press from the pressure source, **PS**. The synthetic mixture is pumped from the syringe pump into the equilibrium cell, **EC**. A vacuum pump, **VP**, attached to the transfer line between the syringe pump and the equilibrium cell is used to evacuate the equilibrium cell or the syringe pump prior to either being filled with the synthetic mixture. The temperature of the syringe pump is maintained below the measurement temperature to ensure that no flashing occurs therein. This is performed with a jacket encasing the pump reservoir. The ethanol contained inside of this jacket is circulated from a constant temperature bath, **WB**, which ensures that the temperature remains constant.

The equilibrium cell is constructed of a sapphire tube, with an ID of 12.7 mm, and a length of 30.03 mm. This sapphire tube is enclosed on either end by titanium flanges. This gives the cell an internal volume of approximately 3.8 cm<sup>3</sup>. A dead volume of about 0.3 cm<sup>3</sup> ( $\pm 10\%$ ) is introduced by the static configuration of the cell. The equilibrium cell is housed within a

France Etuves XU 125 air thermostat, **AT**, which is used to control the temperature of the cell. The contents of the equilibrium cell are observed through a window in the air thermostat wall. A lamp that is placed inside of the air thermostat provides sufficient illumination to observe the phase changes occurring within the cell.

The temperature of the contents of the cell are monitored with a platinum resistance temperature probe, **TP**, which is inserted into the cell, through the top flange. This temperature probe, a Type 5187A probe supplied by Tinsley Precision Instruments, is positioned within the cell such that the tip is positioned along the central axis of the sapphire tube, extending approximately to the centre of the cell. The pressure of the fluid inside of the cell is measured with a Druck PTX 611 pressure transducer, **PT**, with a range of 0 to 16 MPa. This pressure transducer is maintained at a constant temperature by a West 6100 PID controller, **TR**, which controls the temperature of a heating cartridge housed with the pressure transducer at  $T = 373$  K. The analogue signals from the temperature probe and the pressure transducer, obtained by an Agilent 34401A data acquisition unit, **DAU**, are converted into digital signals, and are logged on a PC, **DAS**.

The fluid from the syringe pump enters into the equilibrium cell through ports machined into the bottom flange. The fluid exits the cell from a similar port machined into the top flange. Thus, all fluid that exits the cell must be in the vapour or supercritical phase. From the equilibrium cell, the fluid flows through a series of valves and is vented in a fume hood.

The temperature probe was calibrated against a 25  $\Omega$  Hart Scientific N° 1678 standard for the temperature range of  $T = (296.36 \text{ to } 486.65)$  K. This standard was calibrated by the Laboratoire National d'Essais (Paris). The temperature standard calibration had a standard deviation of 0.039 K, and the correlation of the calibration of the Tinsley Precision Instruments probe introduced a further 0.02 K uncertainty. The pressure transducer was

calibrated for the measurement of pressures of between (0 and 15.5) MPa, against a Druck PACE5000 pressure controller, which was certified by the Laboratoire National d'Essais (Paris) to have a standard deviation of  $1 \times 10^{-3}$  MPa. The calibration correlation itself had an uncertainty of  $3.9 \times 10^{-4}$  MPa.

### ***Experimental Procedure.***

*Static-analytic apparatus.* Initially, a vacuum is pulled in the equilibrium cell and the loading lines at ambient temperature. For binary measurements, two thermal presses are loaded with each pure component, and attached to the loading lines. The equilibrium cell is then lowered into the constant temperature bath.

When the equilibrium temperature is reached, an amount of approximately  $5 \text{ cm}^3$  of the heavier component is introduced into the cell. The equilibrium temperature is deemed to have been reached when the two temperature probes give the same temperature reading (within limits of uncertainty) for at least 10 minutes. After loading, the vapour pressure of the pure component is measured at the equilibrium temperature [12].

After the vapour pressure has been measured, a small volume of the second component is introduced into the cell, and the mixture is allowed to equilibrate. For VLE measurements, equilibrium is assumed to be reached inside of the cell when the pressure does not change by more than 1 kPa for a period of at least 10 minutes, while stirring continuously [12]. Once equilibrium is attained, the conditions (pressure, temperature and compositions of the phases) are measured. Thereafter, a further small volume of the second component is added into the cell, and the process is repeated. This process is continued until such a time as successive equilibrium mixtures have provided sufficient co-existence points to cover the two-phase envelope. With the measurements at subcritical conditions (for both components), the two-

phase envelope can be traversed in both directions, starting with either of the pure components.

For each equilibrium measurement, at least six samples of both the vapour and the liquid phases are taken using the ROLSI<sup>TM</sup> capillary sampler. These are analysed to verify the repeatability of the composition measurements. The criterion for the acceptance of the measured phase composition is that the range of the data points is less than the uncertainty due to the calibration of the gas chromatograph.

*Critical point determination apparatus.* The fluid to be measured is prepared in the volumetric press by the addition of known masses of each component. These masses are measured using a Mettler Toledo XP2004S balance with an uncertainty of 0.7 mg. When mixtures containing n-hexane were being synthesized, the n-hexane was degassed using a vacuum pump prior to being added to the cell. This degassing was performed at a pressures below the vapour pressure of n-hexane at the ambient temperature for approximately 10 minutes.

The prepared mixture is thereafter compressed to approximately 10 MPa in the volumetric press, using the pressure source (high pressure nitrogen). This pressurisation is to ensure that only a single (liquid) phase exists inside of the volumetric press. The liquid is then transferred into the syringe pump, where it is held at a temperature of  $T = 288$  K. To begin the measurements, the cell is filled to approximately half of its volume with the mixture. The cell is then sealed, and the temperature of the air thermostat is increased. The loading of the cell to approximately half of its volume with the mixture was important, as otherwise, upon heating, the fluid could all become a vapour or all become a liquid prior to the critical locus conditions being attained. Were this the case, the phase transition into the supercritical region would not be visible.

The temperature and pressure at which the critical opalescence is observed is recorded, and thereafter the temperature is decreased, recording the conditions at which the critical opalescence occurs once again. This process is repeated twice before the cell is evacuated and a fresh portion of the same mixture is added into the cell. The maximum rate at which the temperature was allowed to change was limited to 0.3 K per minute, in order to prevent sizeable temperature gradients from developing within the cell, due to the poor circulation in the cell caused by no agitation of the cell contents. The mean temperature and pressure, from at least five repeated loadings, are reported as the measured critical locus.

## **Correlations**

*Subcritical data treatment.* The subcritical VLE data was correlated with the Peng-Robinson equation of state (PR EOS) with the classical (van der Waals) mixing rule [14]. The models for each isotherm were fitted to the data using the direct ( $\phi$ - $\phi$ ) data regression approach in Aspen V8.4 [15] using a modified Barker's objective function (minimisation of the pressure and vapour phase composition deviations). The fit of the models to the experimental data were quantified with the mean relative deviations (MRDs) and the absolute average relative deviations (AARDs) for each isotherm [4].

*Critical point determination.* The composition and pressure at the critical point were extrapolated from the experimental data using the method that was proposed by Ungerer et al. [5]. This method uses the extended scaling laws to extrapolate to the critical point for a given isotherm for binary mixtures. The equations representing the extended scaling laws are given by Equations 1 and 2. This technique was further discussed by El Ahmar et al. [16].

$$y - x = \lambda_1 (P_c - P) + \mu (P_c - P)^\beta \quad (1)$$

$$\frac{y + x}{2} - x_c = \lambda_2 (P_c - P) \quad (2)$$

## Discussion

The isothermal vapour-liquid equilibrium (VLE) data of the R-23 + n-propane system were measured at temperatures of between  $T = (283.15 \text{ and } 353.15) \text{ K}$ , using the static-analytic apparatus. The VLE data are given in Tables 3 and 4, and are plotted in Figure 5. The vapour pressures of both R-23 and n-propane were compared to literature data in Figures 3 and 4. There was good agreement between the experimental data and that available in literature for R-23 [4, 17-19], with differences between the experimental data and the literature data of less than 0.3%, and for n-propane [7, 8, 20-22], with deviations of less than 0.5% between the experimental and the literature data. Due to the large volumes of vapour pressure data that were available for n-propane, several authors that provided data over the range of temperatures that were investigated in this study were utilised, rather than using the entire n-propane vapour pressure dataset. The  $T = (293.15 \text{ and } 313.15) \text{ K}$  isotherms were compared to the data that were measured by Ju et al. [7], which are also included in Figure 5. Figure 6 provides an enlargement of the plot for compositions of R-23 between (0.7 and 1.0) mole fraction, to enable a better view of the fit of the models and extrapolated data to the measured data.

The temperature independent PR EOS model with classical (van der Waals) mixing rule was fitted to each isothermal set of VLE data. The temperature independent binary interaction parameters for the model are provided in Table 5. These parameters are also plotted against the temperature in Figure 7. There was a good fit of the models to the experimental data, with most of the MRDs and AARDs being below 2 %. A second order polynomial fitted to the parameters suggests a temperature dependence of the parameters that is not linear.

The critical loci that were measured using the critical locus determination apparatus for the systems of R-23 + n-propane, R-116 + n-propane, and R-23 + n-hexane, are reported alongside their uncertainties in Table 6. The critical loci extrapolated from subcritical VLE data for the R-23 + n-propane, and R-116 + n-propane [8] systems using the method of Ungerer et al. [5, 16] are reported in Table 7. Redlich-Kister (RK) type correlations were fitted to the  $T$ - $x$  and  $P$ - $x$  projections of the critical locus curves for all three systems. The parameters for different order correlations used to depict the  $T$ - $x$  projection of the critical locus curve are given in Table 8, alongside the MRDs. The order of the correlation was selected such that the deviation between the measured value and the correlated value was less than the experimental uncertainty. Table 9 lists the parameters for the correlations of the  $P$ - $x$  projection. The correlations were better able to describe the  $T$ - $x$  projection than the  $P$ - $x$  projection, with the MRDs of less than 2% for temperature, but substantially higher for pressure. The mixture critical pressures were not well described even by a 4<sup>th</sup> order polynomial for the R-23 + n-hexane system.

The  $P$ - $x$  and  $T$ - $P$  projections of the R-23 + n-propane critical locus curve are presented in Figures 8 and 9, respectively. There is a fairly close agreement between the critical loci that were measured directly and those that were extrapolated from the VLE data. The RK type correlations are capable of providing a rough description of the critical locus curve, with the 3<sup>rd</sup> order correlation possibly providing the closest fit. The 4<sup>th</sup> order correlation was not

suitable for this system. It behaved in a similar manner to how an over-specified model would be expected to behave. The vapour pressure data for R-23 and n-propane were plotted using the PR-MC [23] parameters reported by Williams-Wynn et al. [4] and Ramjugernath et al. [8], respectively. The inflection of the critical locus curve at a minimum pressure, and the subsequent crossing of the vapour pressure curve, near to the pure R-23 critical point ( $T = 299.07$  K) is indicative of the negative azeotrope which occurs for the R-23 + n-propane system.

The  $P$ - $x$  projection of the R-116 + n-propane critical locus curve was plotted on Figure 10 alongside the VLE data that were measured for this system by Ramjugernath et al. [8]. The data of Ramjugernath were extrapolated to the critical loci by using the technique of Ungerer et al. [5]. These critical loci are also included on Figure 10 alongside the RK-type correlation curves which were fitted to the experimental data. There was good agreement between the experimentally measured and the extrapolated critical loci. The  $T$ - $P$  projection of the critical locus curve (Figure 11) confirms this excellent agreement. The first order correlation of the  $T$ - $P$  curve is not capable of adequately describing the critical locus curve, however, the 2<sup>nd</sup> order and higher correlations do provide good descriptions.

The  $P$ - $x$  projection of the critical loci for the R-23 + n-hexane system measured directly with the critical point determination apparatus are plotted on Figure 12. The VLE data and the section of the critical locus curve that was calculated using the method of Heidemann and Khalil [6] from the work of Williams-Wynn et al. [4] are also included on this plot. The RK-type correlations of the critical locus curve are also included in Figure 12. This  $P$ - $x$ - $y$  plot is enlarged for compositions of between (0.7 and 1.0) mole fraction in Figure 13. Figure 14 projects the critical locus curve for this system onto the  $T$ - $P$  axis. The RK-type correlations were not capable of adequately describing the critical locus curve indicated by the experimental data. For this system, the mean relative deviation between the experimental

data and the model was 9.2 %, whereas the maximum uncertainty of the measurements was 1.3 %. In addition, there were substantial differences between the experimentally measured critical loci and the extrapolated critical loci. This indicates that either the extrapolation technique is not sufficiently accurate, or, alternatively, the lack of stirring mechanism within the critical locus measurement apparatus translated into inaccuracies in the critical loci that were measured. The curve that was calculated from the thermodynamic models used by Williams-Wynn et al. [4], by the method of Heidemann and Khalil follows the extrapolated data fairly closely. This is because both techniques rely on the sub-critical co-existence data.

The R-23 + n-propane system does not appear to exhibit a three phase region, and therefore, based upon the  $T$ - $P$  plot for this system, it would appear to be a van Konynenberg and Scott (VKS) [24] type I-A system. There is however, the possibility that the upper critical end point (UCEP) occurs at temperatures below those measured in this study. If this is the case, then the system would be a VKS type II-A system. The azeotrope that is present for this system lends to the addition of the ‘A’ suffix. The R-23 + n-hexane system exhibits a three phase region, but also only a single critical curve traversing between the two pure component critical points. Thus this system is classified as a type II system. The R-116 + n-propane system exhibits similar characteristics to the R-23 + n-propane system, and is therefore also classified as either VKS type I-A or type II-A.

## Conclusions

The isothermal VLE data for the R-23 + n-propane system were measured using a static-analytic apparatus at temperatures of between  $T = (293.18 \text{ and } 353.15) \text{ K}$ . The PR EOS with classical mixing rules was used to model this experimental data independent of temperature. A good description of the experimental data was achieved with this single parameter model. It was, however, shown that the binary interaction parameters were not linearly dependent on

temperature. Several critical loci were extrapolated from subcritical VLE data. These extrapolated loci were compared with measured critical loci. These measurements were performed using a ‘critical loci determination apparatus’. The extrapolated data and the experimental data showed close agreement. Critical loci were also measured using the apparatus for the systems of R-116 + n-propane and R-23 + n-hexane. The critical locus curves were modelled with Redlich-Kister type correlations, which were fitted to the experimental data. The correlations were capable of providing a good fit of the systems containing n-propane, however, with the system with n-hexane, they did not exhibit the same ability. Lastly, the critical locus curve, calculated from the thermodynamic model fitted to R-23 + n-hexane VLE data by Williams-Wynn et al. [4], by the technique of Heidemann and Khalil, was compared with the experimental and extrapolated data. The extrapolated data and the calculated data showed similar trends. This was presumably due to both originating from the reported VLE data. The (R-23 or R-116) + n-propane binary mixtures were both classified as either type I-A or II-A systems. The binary R-23 + n-hexane mixture was classified as a type II system.

## **Acknowledgement**

This work was supported by the South African Research Chairs Initiative of the Department of Science and Technology of South Africa and the National Research Foundation. The authors also wish to acknowledge the Institut Carnot M.I.N.E.S. for their support in this study.

## References

- [1] Sheng, Y. J.; Chen, P. C.; Chen, Y. P.; Wong, D. S. H., **1992**. *Ind. Eng. Chem. Res.*, 31(3), 967-973.
- [2] Gil, L.; Blanco, S. T.; Rivas, C.; Laga, E.; Fernández, J.; Artal, M.; Velasco, I., **2012**. *J. Supercrit. Fluids*, 71, 26-44.
- [3] Dobbs, J. M.; Wong, J. M.; Johnston, K. P., **1986**. *J. Chem. Eng. Data*, 31(3), 303-308.
- [4] Williams-Wynn, M. D.; Naidoo, P.; Ramjugemath, D., **2016**. *J. Chem. Thermodyn.*, 94, 31-42.
- [5] Ungerer, P.; Tavitian, B.; Boutin, A., **2005**. *Applications of Molecular Simulation in the Oil and Gas Industry- Monte Carlo Methods*. IFP Publications: Paris, France,
- [6] Heidemann, R. A.; Khalil, A. M., **1980**. *AIChE J.*, 26(5), 769-779.
- [7] Ju, M.; Yun, Y.; Shin, M. S.; Kim, H., **2009**. *J. Chem. Thermodyn.*, 41(12), 1339-1342.
- [8] Ramjugernath, D.; Valtz, A.; Coquelet, C.; Richon, D., **2009**. *J. Chem. Eng. Data*, 54(4), 1292-1296.
- [9] Ramjugemath, D.; Valtz, A.; Richon, D.; Williams-Wynn, M. D.; Coquelet, C., **2015**. *J. Chem. Eng. Data*, not published.
- [10] Guilbot, P.; Valtz, A.; Legendre, H.; Richon, D., **2000**. *Analisis*, 28, 426-431.
- [11] Juntarachat, N.; Valtz, A.; Coquelet, C.; Privat, R.; Jaubert, J.-N., **2014**. *International Journal of Refrigeration*, 141-152.
- [12] Valtz, A.; Coquelet, C.; Baba-Ahmed, A.; Richon, D., **2003**. *Fluid Phase Equilib.*, 207, 53-67.
- [13] Soo, C.-B.; Théveneau, P.; Coquelet, C.; Ramjugernath, D.; Richon, D., **2010**. *J. Supercrit. Fluids*, 55(2), 545-553.
- [14] Peng, D. Y.; Robinson, D. B., **1976**. *Ind. Eng. Chem. Fundam.*, 15, 59-64.
- [15] Aspen Technology *Aspen Plus V8.4*. 2012.
- [16] El Ahmar, E.; Valtz, A.; Naidoo, P.; Coquelet, C.; Ramjugernath, D., **2011**. *J. Chem. Eng. Data*, 56(5), 1918-1924.
- [17] Hou, Y. C.; Martin, J. J., **1959**. *AIChE J.*, 5(1), 125-129.
- [18] Rasskazov, D. S.; Petrov, E. K.; Spiridonov, G. A.; Ushmajkin, E. R., **1975**. *Teplofiz. Svoistva Veshchestv Mater.*, 8, 4-16.
- [19] Hori, K.; Okazaki, S.; Uematsu, M.; Watanabe, K. *An Experimental Study of Thermodynamic Properties of Trifluoromethane*. Proc. Symp. Thermophys. Prop. 1982. Gaithersburg: ASME.
- [20] Dong, X.; Gong, M.; Liu, J.; Wu, J., **2011**. *The Journal of Chemical Thermodynamics*, 43(3), 505-510.
- [21] Sage, B. H.; Schaafsma, J. G.; Lacey, W. N., **1934**. *Industrial & Engineering Chemistry*, 26(11), 1218-1224.
- [22] Thomas, R. H. P.; Harrison, R. H., **1982**. *Journal of Chemical & Engineering Data*, 27(1), 1-11.
- [23] Mathias, P. M.; Copeman, T. W., **1983**. *Fluid Phase Equilib.*, 13, 91-108.
- [24] van Konynenburg, P. H.; Scott, R. L., **1980**. *Philos. Trans. R. Soc. London, Ser. A*, 298, 495-540.
- [25] Lide, D. R., **2004**. *Crc Handbook of Chemistry and Physics 2004-2005*. CRC Press LLC: Boca Raton, USA,
- [26] *Dortmund Data Bank (Ddb)*, 2012, DDBST Software and Separation Technology GmbH: Oldenburg, Germany.

- [27] NIST ThermoData Engine, *Nist Thermodata Engine 103b - Pure Compounds, Binary Mixtures, and Chemical Reactions*, Thermodynamics Research Centre, Editor 2013: Boulder, CO, USA.

**Table 1.** Chemical suppliers, CAS numbers and stated purities

	Supplier	CAS Number	Stated Purity
<b>Trifluoromethane,</b> R23, CHF <sub>3</sub> <sup>a</sup>	Climalife	75-46-7	0.995 <sup>b</sup>
<b>Hexafluoroethane,</b> R116, C <sub>2</sub> F <sub>6</sub> <sup>a</sup>	Air Liquide	76-16-4	0.99999 <sup>b</sup>
<b>n-Propane,</b> C <sub>3</sub> H <sub>8</sub> <sup>a</sup>	Messer	74-98-6	0.99995 <sup>b</sup>
<b>n-Hexane,</b> C <sub>6</sub> H <sub>14</sub>	Sigma-Aldrich	110-54-3	0.99 <sup>c</sup>

<sup>a</sup> Further purification of components was not undertaken.

<sup>b</sup> volumetric (molar) basis

<sup>c</sup> mass basis

**Table 2.** Critical properties from literature data

	$T_c/K$	$P_c/MPa$	$\omega$
<b>Trifluoromethane,</b> R23, $CHF_3$ <sup>a</sup>	299.07 <sup>a</sup>	4.836 <sup>a</sup>	0.264 <sup>c</sup>
<b>Hexafluoroethane,</b> R116, $C_2F_6$	293.04 <sup>b</sup>	3.042 <sup>b</sup>	0.229 <sup>b</sup>
<b>n-Propane,</b> $C_3H_8$	369.95 <sup>b</sup>	4.246 <sup>b</sup>	0.152 <sup>b</sup>
<b>n-Hexane,</b> $C_6H_{14}$	507.40 <sup>b</sup>	3.014 <sup>b</sup>	0.301 <sup>c</sup>

<sup>a</sup> Ref. [25]<sup>b</sup> Ref. [26]<sup>c</sup> Ref. [27]

**Table 3.** P-x-y data for the R-23 (1) + n-propane (2) system at temperatures below the critical temperature of R-23.

$T = 293.18 \text{ K}^a$			$T = 298.15 \text{ K}^a$		
$P/\text{MPa}^b$	$x_1^c$	$y_1^d$	$P/\text{MPa}^b$	$x_1^e$	$y_1^f$
0.8368	0	0	0.9508	0	0
1.3538	0.053	0.341	1.6831	0.075	0.387
1.8594	0.120	0.508	3.0651	0.314	0.648
2.8118	0.322	0.670	2.3621	0.170	0.550
3.1979	0.453	0.717	3.6164	0.484	0.709
3.6002	0.625	0.769	3.9604	0.610	0.747
3.7345	0.687	0.792	4.2464	0.720	0.788
3.9258	0.776	0.830	4.4949	0.819	0.841
4.1419	0.906	0.915	4.5411	0.840	0.854
4.1703	0.937	0.940	4.5644	0.850	0.862
4.1769	0.948	0.949	4.6067	0.871	0.878
4.1800	0.954	0.955	4.6287	0.883	0.888
4.1774	-	0.955	4.6686	0.906	0.906
4.1797	0.959	0.960	4.6944	0.927	0.927
4.1819	0.966	0.967	4.7180	0.957	0.957
4.1823	0.970	0.970	4.7191	0.964	0.964
4.1821	0.974	0.974	4.7206	0.968	0.968
4.1822	0.977	0.977	4.7184	-	0.962
4.1805	0.982	0.982	4.7217	0.980	0.979
4.1790	0.986	0.986	4.7208	0.988	0.988
4.1787	0.992	0.991	4.7093	1	1
4.1717	1	1			

Uncertainties, calculated with  $k = 2$  are as follows:

<sup>a</sup>  $U(T) = 0.08 \text{ K}$ ,

<sup>b</sup>  $U(P) = 0.0008 \text{ MPa}$ ,

<sup>c</sup>  $U(x_1) = 0.008$ ,

<sup>d</sup>  $U(y_1) = 0.009$ ,

<sup>e</sup>  $U(x_1) = 0.009$ ,

<sup>f</sup>  $U(y_1) = 0.008$ .

**Table 4.**  $P$ - $x$ - $y$  data for the R-23 (1) + n-propane (2) system at temperatures above the critical temperature of R-23.

$T = 313.15 \text{ K}^a$			$T = 323.15 \text{ K}^a$			$T = 353.15 \text{ K}^a$		
$P/\text{MPa}_b$	$x_1^c$	$y_1^d$	$P/\text{MPa}_b$	$x_1^c$	$y_1^d$	$P/\text{MPa}_b$	$x_1^e$	$y_1^f$
1.3801 <sup>g</sup>	0	0	1.7130	0	0	3.1354	0	0
2.0388	0.057	0.274	2.2264	0.040	0.182	3.4204	0.018	0.048
3.0674	0.173	0.481	2.4390	-	0.237	3.5010	0.025	0.063
3.7409	0.278	0.558	2.4525	0.060	0.239	3.7949	0.046	0.104
4.1408	0.354	0.592	2.8503	0.097	0.327	4.0015	0.062	0.133
4.6054	0.460	0.623	3.1572	0.128	0.374	4.2831	0.085	0.163
4.8038	0.512	0.629	3.5130	-	0.418	4.3708	0.092	0.170
4.9324	0.550	0.630	3.5541	0.172	0.431	4.4198	0.096	0.173
5.0006	0.576	0.623	4.0748	-	0.485	4.5218	0.105	0.182
			4.1810	0.257	0.491	4.6256	0.115	0.189
			4.4982	0.307	0.505	4.7208	0.125	0.195
			4.8326	0.366	0.523			
			5.0287	0.406	0.530			
			5.1504	0.437	0.527			
			5.1895	0.447	0.523			

Uncertainties, calculated with  $k = 2$  are as follows:

<sup>a</sup>  $U(T) = 0.08 \text{ K}$ ,

<sup>b</sup>  $U(P) = 0.001 \text{ MPa}$ ,

<sup>c</sup>  $U(x_1) = 0.009$ ,

<sup>d</sup>  $U(y_1) = 0.009$ ,

<sup>e</sup>  $U(x_1) = 0.004$ ,

<sup>f</sup>  $U(y_1) = 0.005$ .

<sup>g</sup>  $U(P) = 0.01 \text{ MPa}$

**Table 5.** Model results for the PR EOS with the van der Waals mixing rules for the system of R-23 (1) + n-propane (2).

	T / K						
	283.15	293.18	298.15	303.15	313.15	323.15	353.15
$k_{12}$	0.2000	0.1981	0.2055	0.2010	0.2105	0.2184	0.2565
MRD ( $P$ ) <sup>a</sup>	-0.01	0.02	-0.24	-0.16	-0.12	0.03	0.05
AARD ( $P$ ) <sup>b</sup>	1.46	1.00	0.93	1.02	0.79	0.58	0.13
MRD ( $y$ ) <sup>a</sup>	1.14	-0.39	-1.55	-0.67	-1.36	-2.17	-1.13
AARD ( $y$ ) <sup>b</sup>	1.29	0.89	1.55	1.87	1.46	2.42	1.57

$$^a \quad MRD(\bar{\theta}) = \frac{100}{N_p} \sum_1^{N_p} \frac{\bar{\theta}_{exp} - \bar{\theta}_{calc}}{\bar{\theta}_{exp}}$$

$$^b \quad AARD(\bar{\theta}) = \frac{100}{N_p} \sum_1^{N_p} \frac{|\bar{\theta}_{exp} - \bar{\theta}_{calc}|}{\bar{\theta}_{exp}}$$

**Table 6.** Experimental critical temperatures,  $T_c$ , and pressures,  $P_c$ , of binary mixtures as a function of the mole fractions,  $x_{1,c}$ , measured using the critical point determination apparatus.

$x_{1,c}$	$U(x_{1,c})^a$	$T_c / \text{K}$	$U(T_c)^a / \text{K}$	$P_c / \text{MPa}$	$U(P_c)^a / \text{MPa}$
<i>R23 (1) + n-propane (2)</i>					
0.071	0.005	364.2	0.6	4.61	0.05
0.221	0.005	351.9	0.4	5.08	0.03
0.325	0.004	342.0	0.6	5.32	0.02
0.326	0.004	342.1	0.4	5.28	0.03
0.434	0.003	331.3	0.6	5.37	0.05
0.569	0.003	313.9	0.4	5.07	0.03
0.624	0.002	311.3	0.5	4.97	0.02
0.706	0.008	306.5	0.8	4.82	0.03
<i>R23 (1) + n-hexane (2)</i>					
0.111	0.005	503.3	0.9	3.66	0.08
0.320	0.004	486.9	0.7	5.34	0.08
0.537	0.003	454.3	1.1	7.91	0.09
0.661	0.002	427.8	0.2	9.18	0.12
0.773	0.002	383.2	1.0	9.82	0.10
0.860	0.002	343.0	0.9	7.98	0.04
0.922	0.002	318.7	0.5	5.95	0.06
0.944	0.002	310.8	0.3	5.41	0.03
<i>R116 (1) + n-propane (2)</i>					
0.071	0.005	362.0	0.3	4.31	0.03
0.179	0.005	348.2	0.1	4.26	0.04
0.259	0.004	338.7	0.3	4.16	0.01
0.411	0.003	323.4	0.2	3.85	0.02
0.521	0.003	313.3	0.2	3.61	0.02
0.752	0.002	298.5	0.2	3.17	0.01

<sup>a</sup> The combined expanded uncertainties of composition, temperature and pressure are calculated using a coverage factor,  $k$ , equal to 2.

**Table 7.** Critical temperatures,  $T_c$ , and pressures,  $P_c$ , of binary mixtures as a function of the mole fractions, extrapolated from sub-critical co-existence points by the Ungerer et al. extrapolation technique.

<i>R23 + n-propane</i> <sup>a</sup>			<i>R116 + n-propane</i> <sup>b</sup>		
$x_{1,c}$	$T_c / \text{K}$	$P_c/\text{MPa}$	$x_{1,c}$	$T_c / \text{K}$	$P_c/\text{MPa}$
0.752	303.15	4.747	0.814	296.23	3.140
0.601	313.15	4.978	0.585	308.21	3.456
0.493	323.15	5.243	0.409	323.19	3.854
0.192	353.15	5.103			

<sup>a</sup> extrapolated from the data provided by Ju et al. [7] and from the data measured in this study.

<sup>b</sup> extrapolated from the work of Ramjugernath et al. [8].

**Table 8.** Parameters ( $a_n$ ) for the Redlich-Kister type correlation describing the  $T$ - $x$  projection of the critical locus curves of the three systems, alongside the mean relative deviation ( $MRD$ ) from each correlation.

<b>System</b>	<b><math>a_1</math></b>	<b><math>a_2</math></b>	<b><math>a_3</math></b>	<b><math>a_4</math></b>	<b><math>a_5</math></b>	<b>100×MRD</b>
	-45.68	-65.50	-	-	-	1.777
<i>R-23 + n-propane</i>	-41.79	-72.51	-41.56	-	-	1.087
	-41.79	-72.51	-41.56	$-3.6 \times 10^{-4}$	-	1.087
	-65.43	-18.43	-	-	-	0.411
<i>R-116 + n-propane</i>	-65.35	-20.20	-3.18	-	-	0.409
	-65.55	-9.67	-14.77	-49.04	-	0.268
	231.58	55.46	-	-	-	7.767
<i>R-23 + n-hexane</i>	235.00	20.28	-124.13	-	-	5.177
	257.23	91.27	-190.70	-256.13	-	1.707
	256.50	94.71	-189.22	-268.95	-9.66	1.608

**Table 9.** Parameters ( $b_n$ ) for the Redlich-Kister type correlation describing the  $P$ - $x$  projection of the critical locus curves of the three systems, alongside the mean relative deviation ( $MRD$ ) from each correlation.

<b>System</b>	<b><math>b_1</math></b>	<b><math>b_2</math></b>	<b><math>b_3</math></b>	<b><math>b_4</math></b>	<b><math>b_5</math></b>	<b><math>100 \times MRD</math></b>
	2.530	-3.763	-	-	-	7.059
<i>R-23 + n-propane</i>	2.719	-4.238	-2.158	-	-	3.445
	2.761	-4.338	-2.443	-0.131	-	3.440
	0.045	-2.352	-	-	-	1.063
<i>R-116 + n-propane</i>	0.028	-1.992	0.711	-	-	0.303
	0.026	-1.941	1.134	0.421	-	0.293
	14.575	13.863	-	-	-	43.944
<i>R-23 + n-hexane</i>	14.081	21.337	10.423	-	-	31.608
	16.218	23.607	-8.816	-23.610	-	22.563
	13.645	25.051	20.658	-23.086	-37.505	9.172

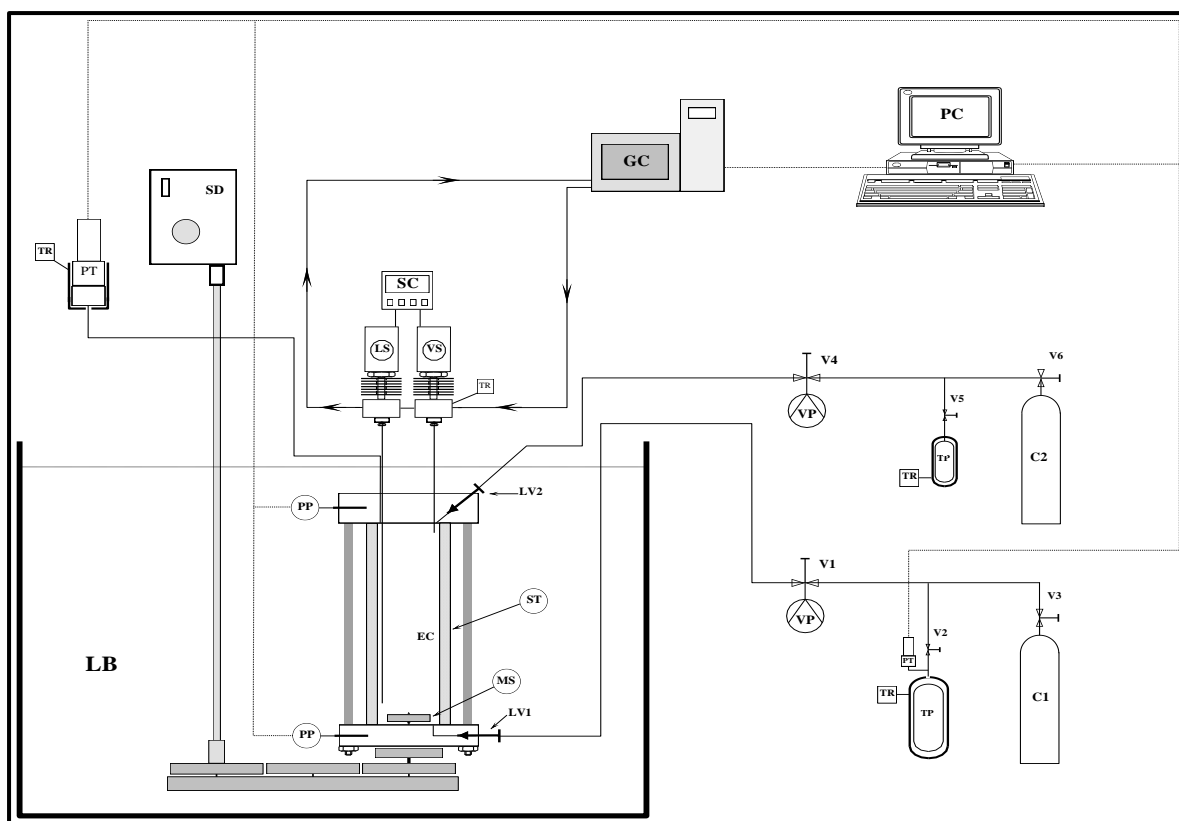


**Figure 1.** Flow diagram of the static-analytic apparatus, as was used by Juntarachat et al. [11]. EC: equilibrium cell; LV: loading valve; MS: magnetic stirrer; PP: platinum resistance thermometer probe; PT: pressure transducer; RT: temperature regulator; LB: liquid bath; TP: thermal press; C1: more volatile compound; C2: less volatile compound; V: valve; GC: gas chromatograph; LS: liquid sampler; VS: vapour sampler; SC: sample controlling; PC: personal computer; VP: vacuum pump.

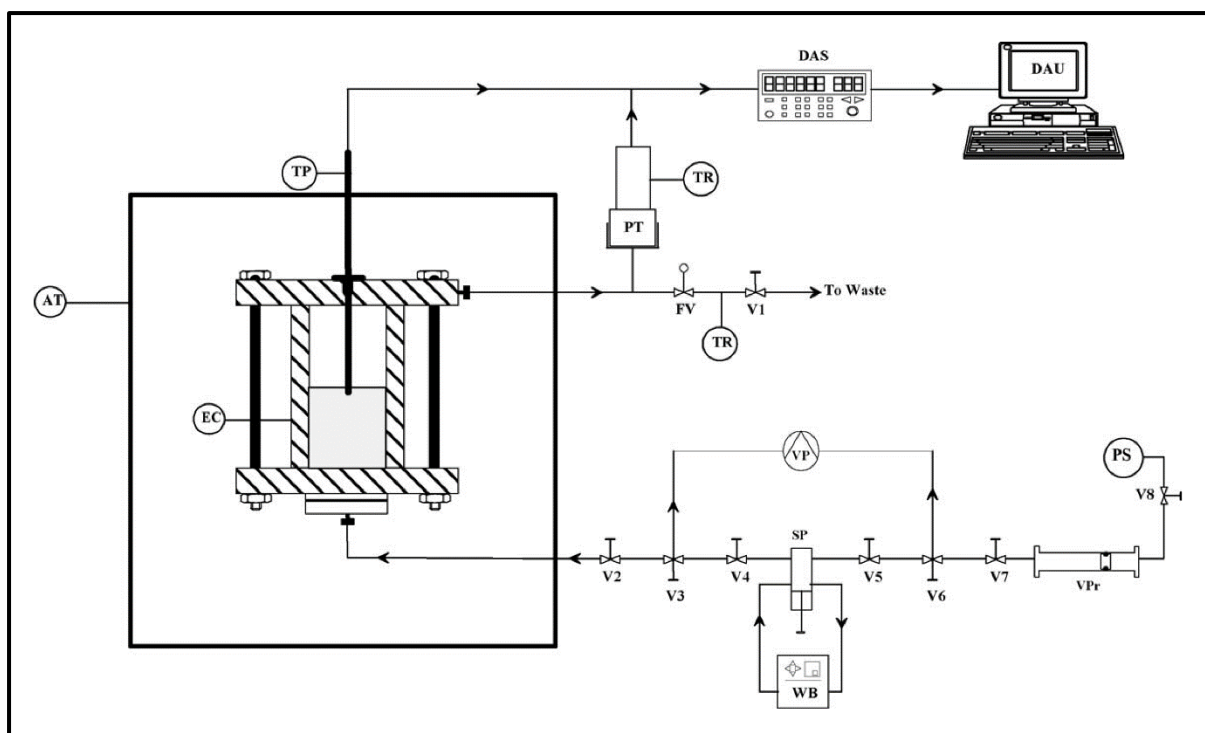


**Figure 2.** Drawing of the critical point determination apparatus modified from the work of Soo et al. [13]. AT, air thermostat; DAS, data acquisition system; DAU, data acquisition unit; EC, equilibrium cell; FV, flow controller valve; PS, pressurisation source; PT, pressure transducer; SP, syringe pump; TP, platinum resistance temperature probe; TR, temperature regulator; V, valve; VP, vacuum pump; VPr, volumetric press; WB, ethanol bath.

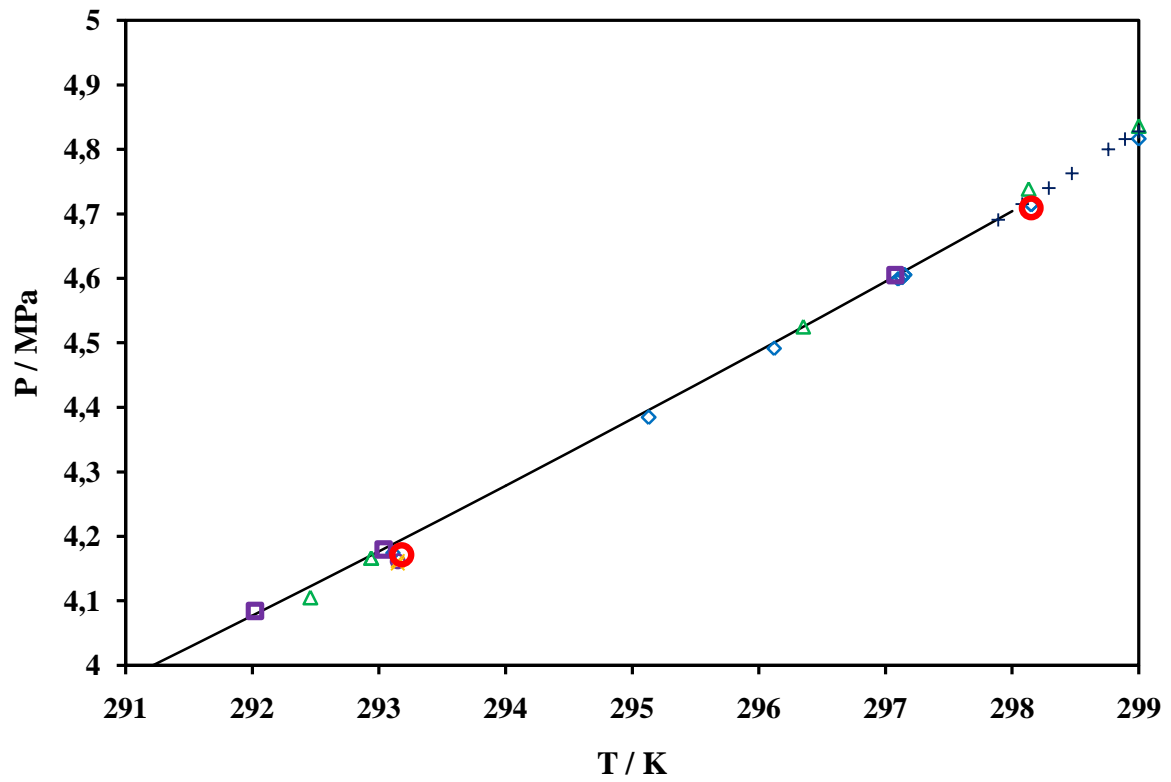


**Figure 3.** Vapour pressure data,  $P$ , for trifluoromethane between temperatures of  $T = (291$  and  $299.07)$  K.  $\bullet$ , experimental data;  $\blacksquare$ , Williams-Wynn et al. [4];  $\blacktriangle$ , Hou and Martin [17];  $\circ$ , Rasskazov et al. [18];  $\blacklozenge$ , Hori et al. [19]; —, PR MC EOS.

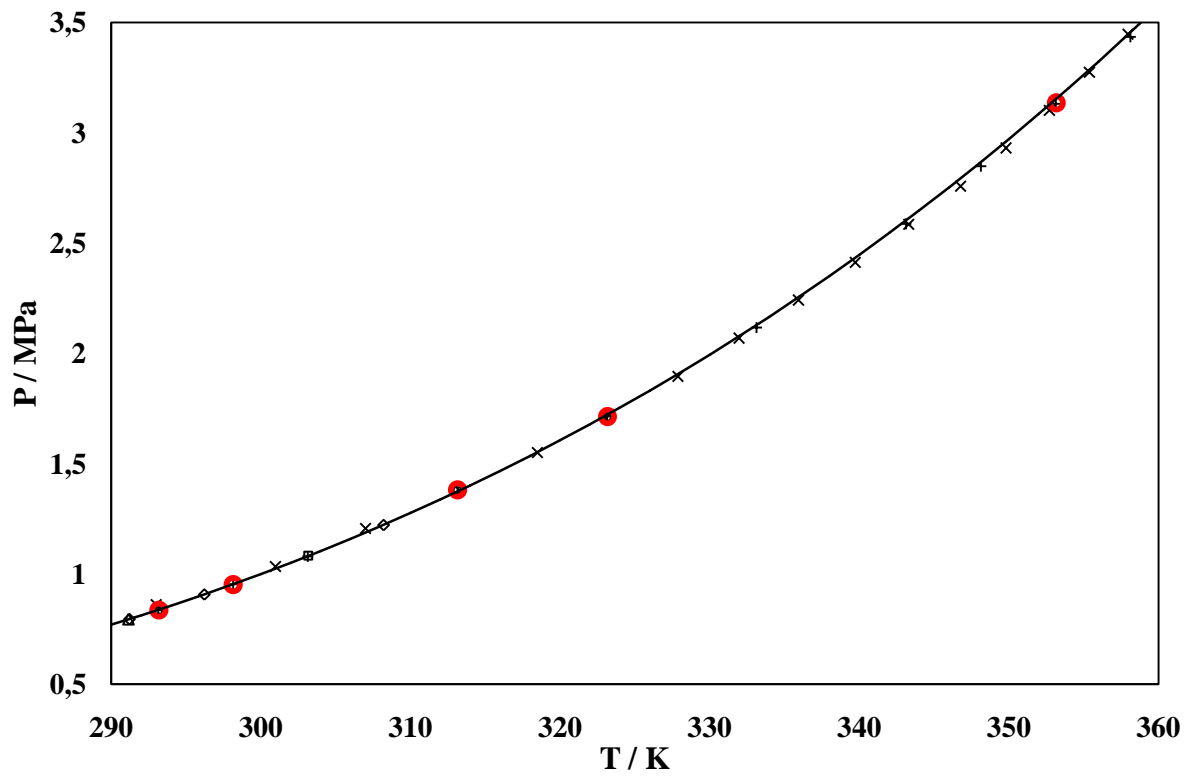


**Figure 4.** Vapour pressure data,  $P$ , for n-propane between temperatures of  $T = (290 \text{ and } 360)$  K. ●, experimental data; □, Ju et al. [7]; ◇, Ramjugernath et al. [8]; ×, Sage et al. [21]; +, Thomas and Harrison [22]; △, Dong et al. [20]. The PR EOS is presented by —.

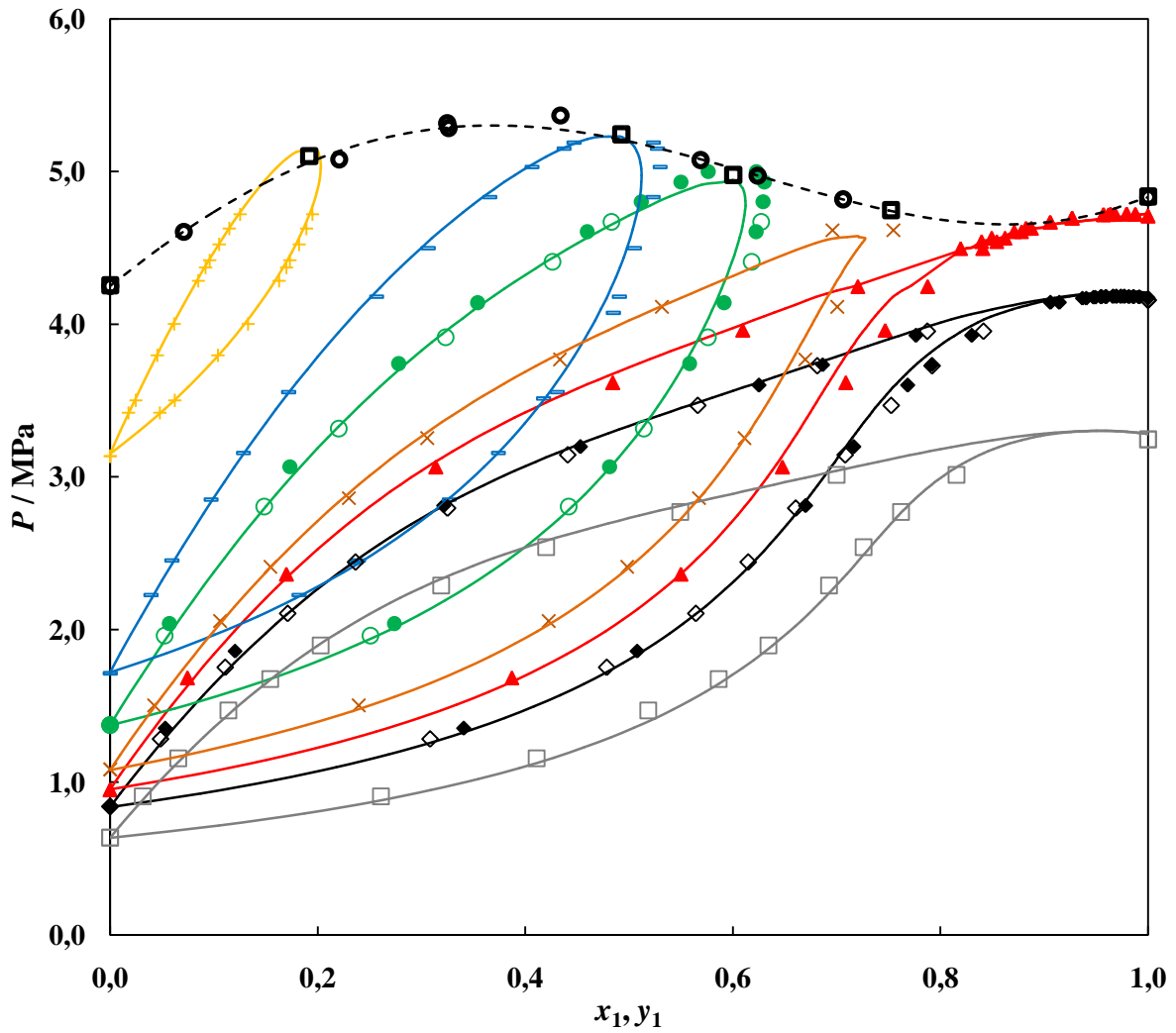


**Figure 5.** Plot of the  $P$ - $x$ - $y$  data for the R23 (1) + n-propane (2) system, with the system critical locus curve. Experimental data at temperatures:  $\blacklozenge$ ,  $T = 293.18$  K;  $\blacktriangle$ ,  $T = 298.15$  K;  $\bullet$ ,  $T = 313.15$  K;  $\blacksquare$ ,  $T = 323.15$  K;  $+$ ,  $T = 353.15$  K. Data modelled with —, PR EOS. Literature data from the work of Ju et al. [8] at given temperatures:  $\square$ ,  $T = 283.15$  K;  $\diamond$ ,  $T = 293.15$  K;  $\times$ ,  $T = 303.15$  K;  $\circ$ ,  $T = 313.15$  K. Critical point modelling:  $\circ$ , extrapolated critical loci;  $\square$ , measured critical loci; - - -, RK 4<sup>th</sup> order correlation.

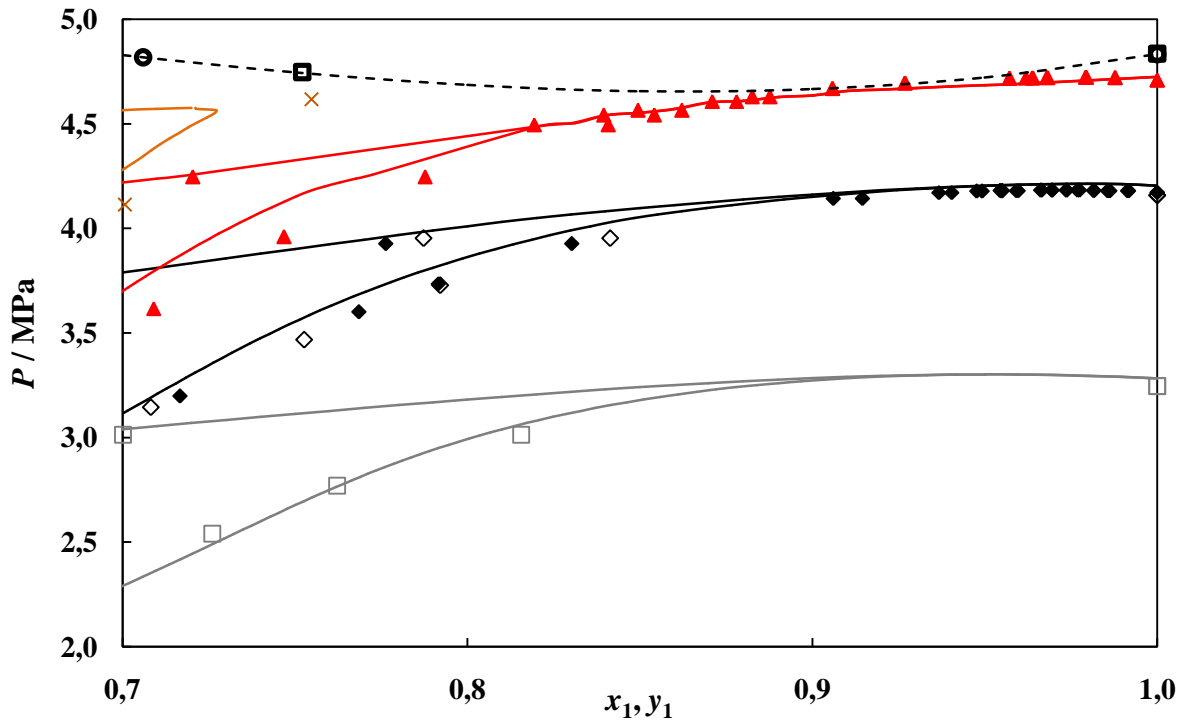


**Figure 6.** Enlarged plot of the  $P$ - $x$ - $y$  data for the R23 (1) + n-propane (2) system, with the system critical locus curve from compositions of (0.7 to 1.0). Experimental data at temperatures  $\blacklozenge$  of:  $\blacklozenge$ ,  $T = 293.18$  K;  $\blacktriangle$ ,  $T = 298.15$  K. Experimental VLE data modelled with: —, PR-EOS models. Literature data from the work of Ju et al. [7]:  $\square$ ,  $\diamond$   $T = 283.15$  K;  $\square$ ,  $T = 293.15$  K;  $\times$ ,  $T = 303.15$  K. Critical point modelling:  $\bullet$ , extrapolated critical loci;  $\square$ , measured critical loci; - - - , RK 4<sup>th</sup> order correlation.

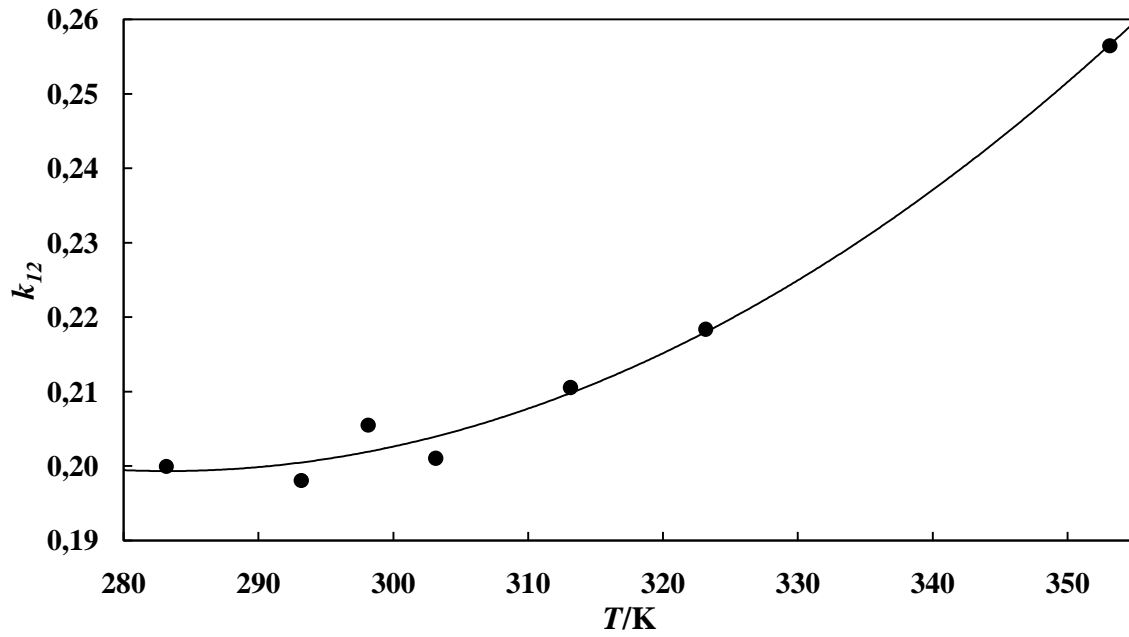


**Figure 7.** Plot of the temperature dependence of the binary interaction parameters for the PR EOS for the system of R-23 (1) + n-propane (2) at temperatures of between  $T = (280$  and  $355)$  K.

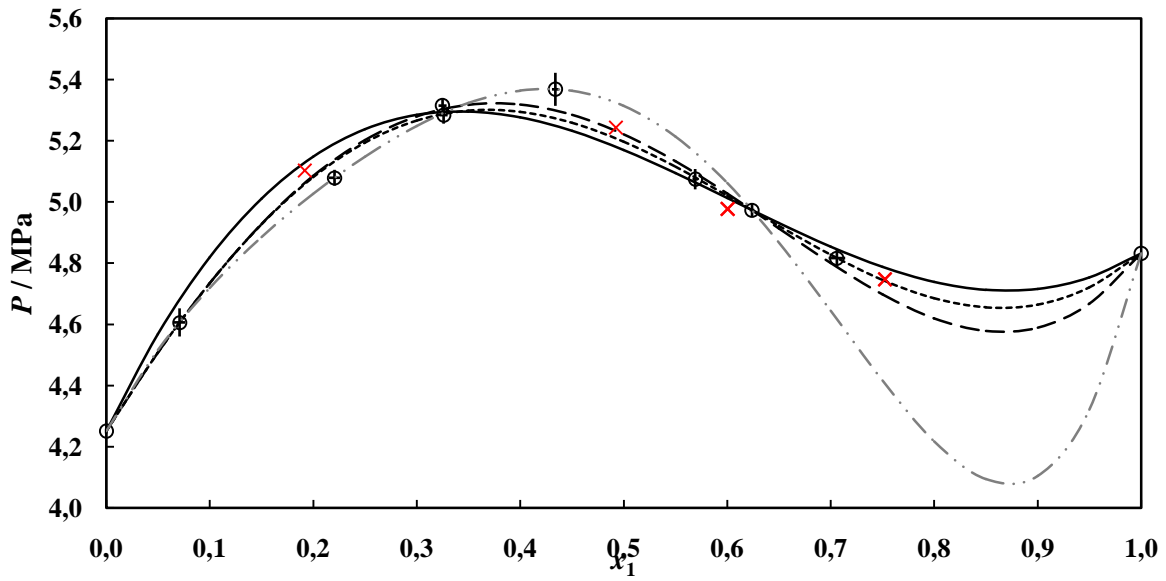


**Figure 8.**  $P$ - $x$  projection of the critical locus curve of R-23 (1) + n-propane (2).  $\circ$ , experimental data with error bars;  $\times$ , critical loci extrapolated from subcritical VLE data; —, 1<sup>st</sup> order RK correlation; - - -, 2<sup>nd</sup> order RK correlation;  $\cdots$ , 3<sup>rd</sup> order RK correlation;  $\cdot$ —, 4<sup>th</sup> order RK correlation.

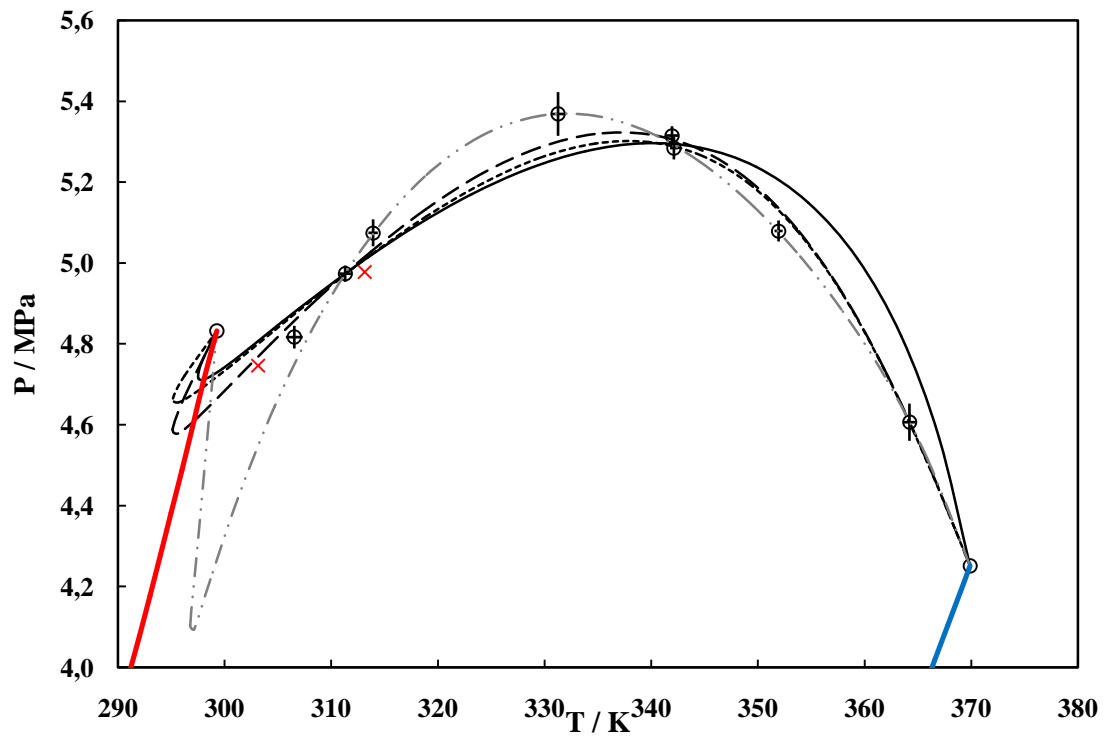


**Figure 9.**  $T$ - $P$  projection of the critical locus curve of R-23 (1) + n-propane (2).  $\circ$ , experimental data with error bars;  $\times$ , critical loci extrapolated from subcritical VLE data. This was modelled with an ‘RK-type’ correlation: —, 1<sup>st</sup> order; - - -, 2<sup>nd</sup> order;  $\cdots$ , 3<sup>rd</sup> order; — · — ·, 4<sup>th</sup> order. Vapour pressure plots from the PR-MC EOS: —, R-23 vapour pressure [4]; —, n-propane vapour pressure [9].

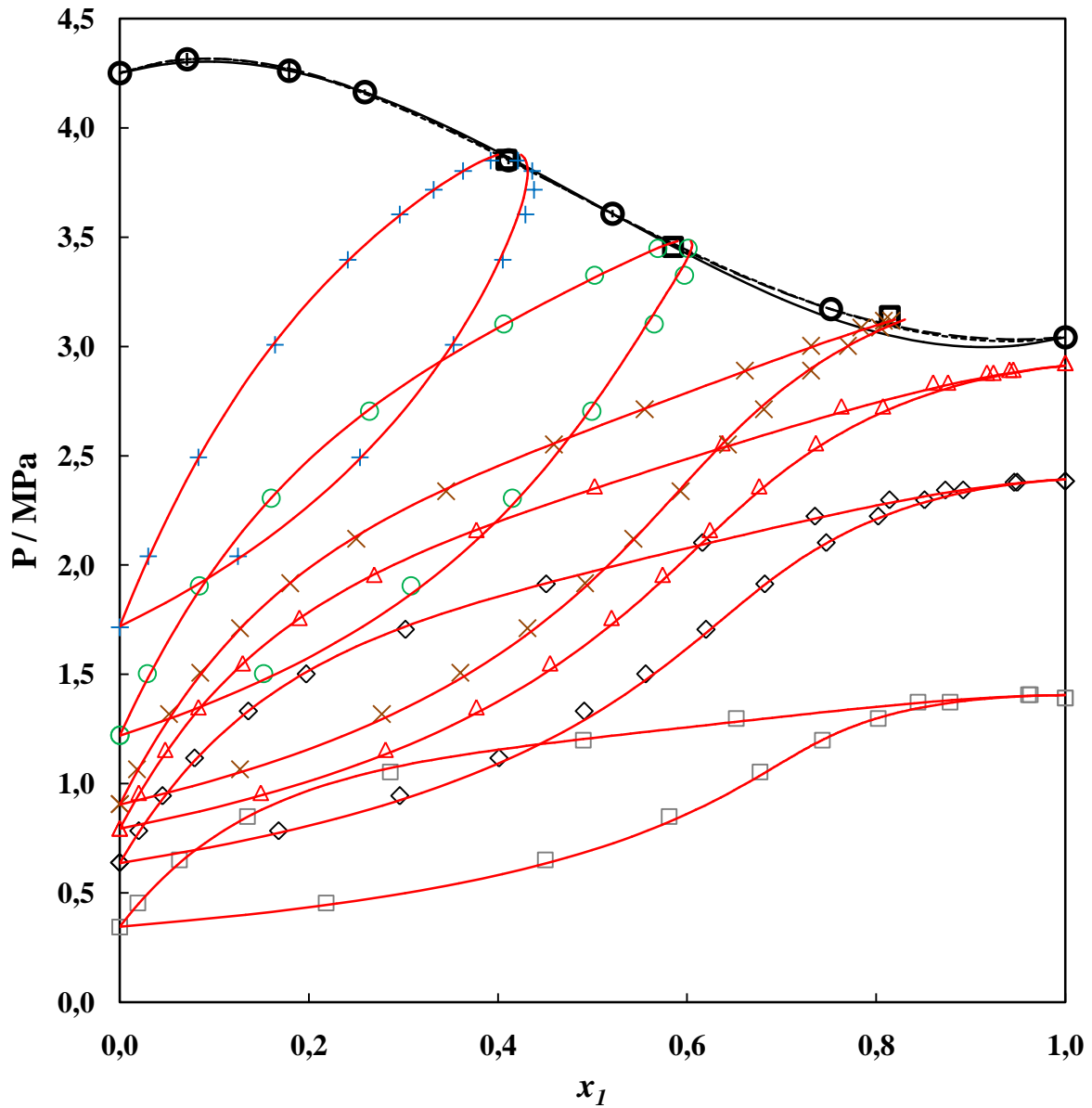


**Figure 10.** Plot of the  $P$ - $x$ - $y$  data for the R116 (1) + n-propane (2) system with the system critical locus curve. Literature data from the work of Ramjugenath et al.[8] at given temperatures of:  $\square$ ,  $T=263.3$  K;  $\diamond$ ,  $T=283.3$  K;  $\triangle$ ,  $T=291.2$  K;  $\times$ ,  $T=296.2$  K;  $\circ$ ,  $T=308.2$  K;  $+$ ,  $T=323.2$  K, and fitted with: —, the PR-MC+WS/NRTL model. Critical loci:  $\blacksquare$ , extrapolated;  $\bullet$ , measured. Critical point modelling with ‘‘RK-type’’ correlations: —, 1<sup>st</sup> order; - - -, 2<sup>nd</sup> order;  $\cdots$ , 3<sup>rd</sup> order.

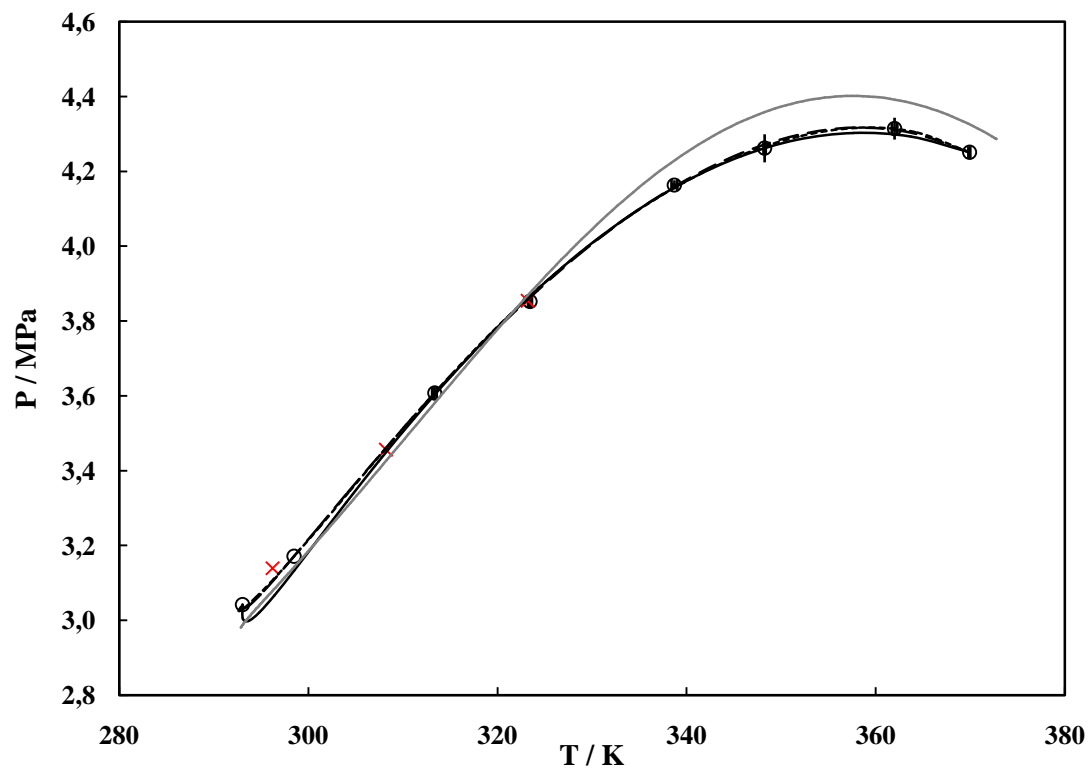


**Figure 11.**  $T$ - $P$  projection of the critical locus curve of R-116 (1) + n-propane (2).  $\circ$ , experimental data with error bars;  $\times$ , critical loci extrapolated from subcritical VLE data; —, 1<sup>st</sup> order RK correlation; - - -, 2<sup>nd</sup> order RK correlation;  $\cdots$ , 3<sup>rd</sup> order RK correlation.

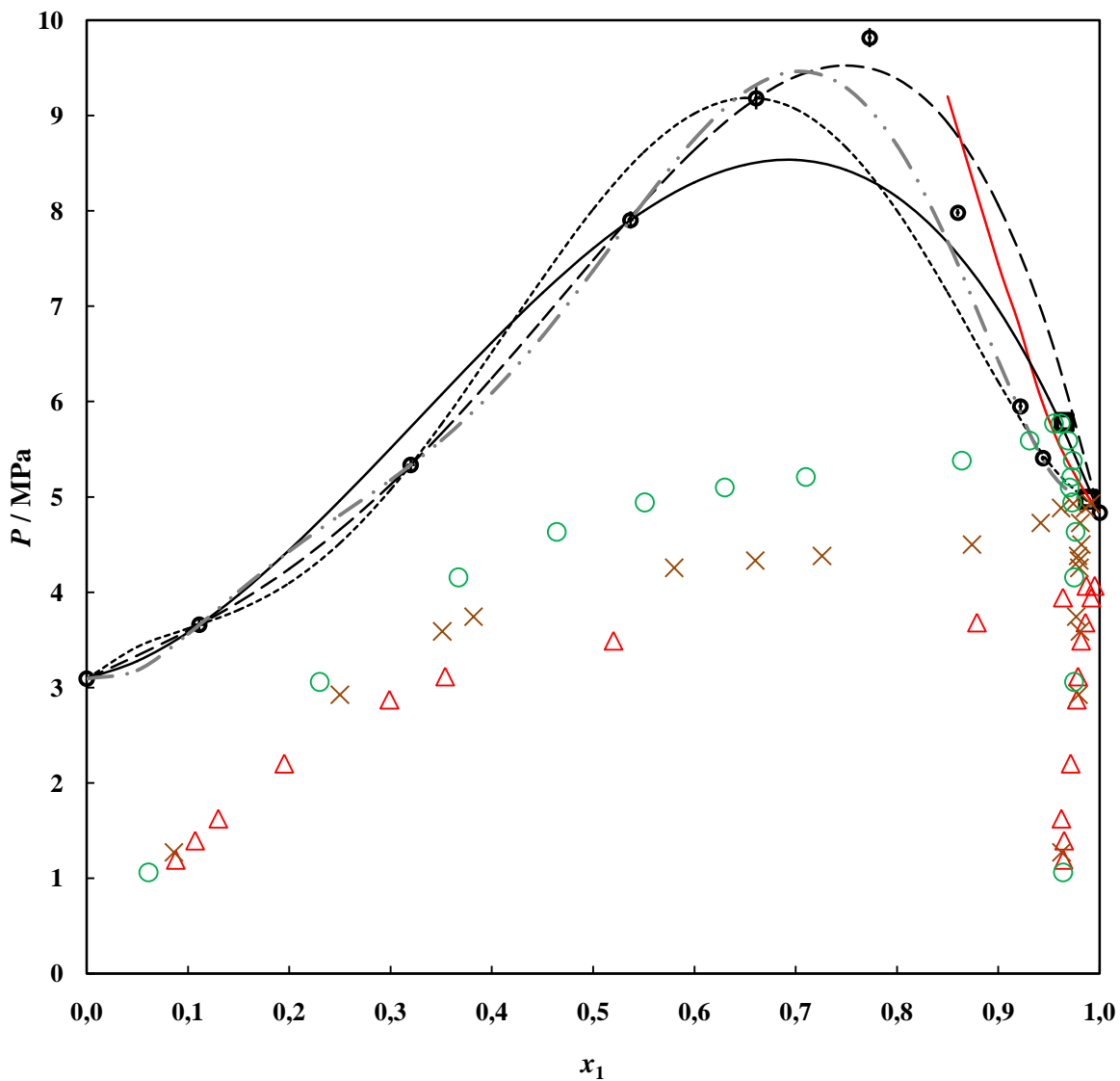


**Figure 12.** Plot of the critical locus curve for the R-23 (1) + n-hexane (2) system, alongside subcritical  $P$ - $x$ - $x$ - $y$  data. Critical  $\blacksquare$  loci:  $\bullet$ ,  $\bullet$  extrapolated;  $\blacksquare$ , measured (including error bars displaying the uncertainties);  $-$ , calculated (by the Heidemann and Khalil method). Modelling of critical locus curves with ‘RK-type’ correlations:  $-$ , 1<sup>st</sup> order;  $- - -$ , 2<sup>nd</sup> order;  $\cdots$ , 3<sup>rd</sup> order;  $\cdot - \cdot -$ , 4<sup>th</sup> order;. Sub-critical VLE data from the work of Williams-Wynn et al. [4] at temperatures:  $\Delta$ ,  $T = 293.0$  K;  $\times$ ,  $T = 303.1$  K;  $\circ$ ,  $T = 313.2$  K.

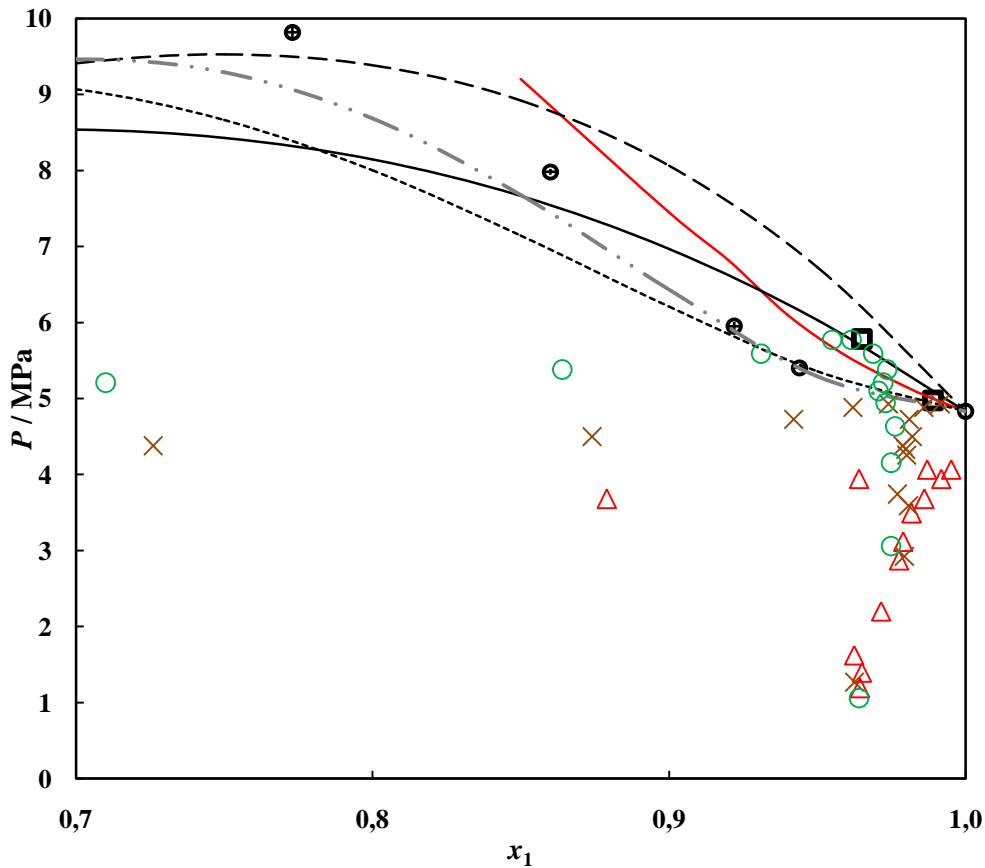


**Figure 13.** Enlarged plot of the critical locus curve for the R-23 (1) + n-hexane (2) system, alongside subcritical  $P$ - $x$ - $y$  data for compositions of between (0.7 and 1.0). Critical  $\blacksquare$  loci:  $\bullet$ ,  $\odot$  extrapolated;  $\oplus$ , measured (including error bars displaying the uncertainties);  $—$ , calculated critical locus curve (by the Heidemann and Khalil method). Critical locus curve modelling with ‘RK-type’ correlations;  $—$ , 1<sup>st</sup> order;  $- - -$ , 2<sup>nd</sup> order;  $\cdots$ , 3<sup>rd</sup> order;  $\cdot - \cdot -$ , 4<sup>th</sup> order. Sub-critical VLE data from the work of Williams-Wynn et al. [4] at temperatures:  $\Delta$ ,  $T = 293.0$  K;  $\times$ ,  $T = 303.1$  K;  $\circ$ ,  $T = 313.2$  K.

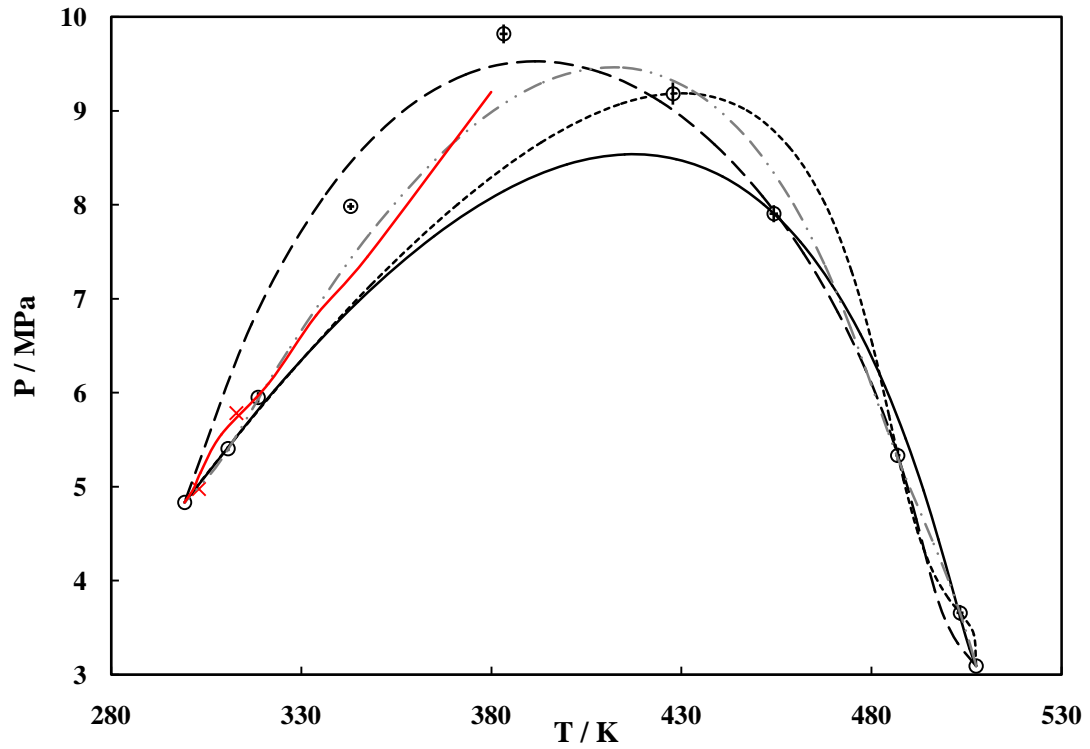


**Figure 14.**  $T$ - $P$  projection of the critical locus curve of R-23 (1) + n-hexane (2).  $\circ$ , experimental data with error bars;  $\times$ , critical loci extrapolated from subcritical VLE data; —, 1<sup>st</sup> order RK correlation; - - -, 2<sup>nd</sup> order RK correlation;  $\cdots$ , 3<sup>rd</sup> order RK correlation,  $\cdot - \cdot -$ , 4<sup>th</sup> order RK correlation.